5992 *Inorg. Chem.* **2010**, *49*, 5992–6004
DOI: 10.1021/ic100547j

Inorganic Chemistry
Article

Self-Assembly of $[Pt_{3n}(CO)_{6n}]^{2-}$ ($n = 4-8$) Carbonyl Clusters: from Molecules to Conducting Molecular Metal Wires

Cristina Femoni, Maria Carmela Iapalucci, Giuliano Longoni, Tatiana Lovato, Stefano Stagni, and Stefano Zacchini*

Dipartimento di Chimica Fisica e Inorganica, Università di Bologna, Viale Risorgimento 4, 40136 Bologna, Italy

Received March 23, 2010

A comprehensive study discussing the different parameters that influence the self-assembly of $[Pt_{3n}(CO)_{6n}]^{2-}$ ($n = 4-8$) clusters with miscellaneous mono- and dications into 0-D, 1-D, 2-D, and 3-D materials is herein reported. As an unexpected bonus, the use of Ru^{II} dications allowed the first structural characterization of the previously unknown $[Pt_{21}(CO)_{42}]^{2-}$ dianion. 0-D structures, which contain isolated ions, are electrical insulators in solid form. Conversely, as soon as infinite chains of clusters are formed, the electrical resistivity, measured in pressed pellets, decreases to 10^5-10^6, 10^4, and 10^2 Ω cm for discontinuous, semicontinuous, and continuous chains, respectively. Therefore, the resemblance of these materials to molecular metal wires is not only morphological but also functional. Preliminary results of possible self-assembly phenomena in a solution of $[Pt_{15}(CO)_{30}]^{2-}$ and $[Pt_{18}(CO)_{36}]^{2-}$ according to dynamic light scattering experiments are also reported.

Introduction

Self-assembly is a phenomenon of paramount importance in several chemical and biological systems that may find applications in bottom-up nanotechnology.[1−3] It is based on the capability of certain molecules to recognize themselves and/or other molecules, which can give rise to the formation of ordered and hierarchical systems. X-ray crystallography studies in the solid state may provide a full and detailed description of the atomic structure of the resulting materials. Conversely, studies in solution usually are more indirect, using techniques (e.g., DLS, SAXS, EXAFS, NMR, etc.) that only give partial information on the structures.[4−6] Dynamic light scattering (DLS) is rather attractive because this technique is experimentally simple, can be applied to almost any kind of sample, and is completely noninvasive.[7] Its major limitation consists of the fact that it measures the hydrodynamic diameter of all species present in solution without any chemical information.

We became interested in the study of self-assembly phenomena while studying the behavior of platinum Chini clusters, $[Pt_{3n}(CO)_{6n}]^{2-}$ ($n = 1-10$).[8−11] All of these molecular species are characterized by stacks of $Pt_3(CO)_3(\mu\text{-}CO)_3$ units along a common C_3 axis and display intratriangular as well as intertriangular Pt−Pt bonds.[8] In previous communications,[10] we have shown that the lowest nuclearity species ($n \leq 4$) crystallize as $[NR_4]^+$ salts systematically adopting ionic 0-D packings,

*To whom correspondence should be addressed. E-mail: zac@ms.fci.unibo.it. Fax: +39 0512093690.

(1) (a) Hornyak, G. L.; Dutta, J.; Tibbals, H. F.; Rao, A. *Introduction to Nanoscience*; CRC Press: Boca Raton, FL, 2008. (b) Ozin, G. A. *Nanochemistry: A Chemical Approach to Nanomaterials*; Royal Society of Chemistry: London, 2009.

(2) (a) Lehn, J. M. *Supramolecular Chemistry: Concepts and Perspective*; Wiley-VCH: New York, 1995. (b) Lehn, J. M. *Angew. Chem., Int. Ed.* **1990**, *29*, 1304. (c) Ruben, M.; Lehn, J. M.; Muller, P. *Chem. Soc. Rev.* **2006**, *35*, 1056.

(3) (a) Mathias, J. P.; Stoddart, J. F. *Chem. Soc. Rev.* **1992**, *21*, 215. (b) Long, D. L.; Cronin, L. *Chem.—Eur. J.* **2006**, *12*, 3698. (c) Whitesides, G. M.; Mathias, J. P.; Seto, C. T. *Science* **1991**, *254*, 1312.

(4) Beyer, G. L. *Physical Methods in Chemistry*; Weissberger, A., Rossiter, B. W., Eds.; Wiley-Interscience: New York, 1971.

(5) (a) Macchioni, A.; Ciancaleoni, G.; Zuccaccia, C.; Zuccaccia, D. *Chem. Soc. Rev.* **2008**, *37*, 479. (b) Macchioni, A. *Chem. Rev.* **2005**, *105*, 2039. (c) Frank, P.; Benfatto, M.; Hedman, B.; Hodgson, K. O. *Inorg. Chem.* **2008**, *47*, 4126. (d) Choppin, G. R.; Thakur, P.; Mathur, J. N. *Coord. Chem. Rev.* **2006**, *250*, 936.

(6) (a) Kratky, C.; Farber, G.; Gruber, K.; Wilson, K.; Dauter, Z.; Nolting, H. F.; Konrat, R.; Krautler, B. *J. Am. Chem. Soc.* **1995**, *117*, 4654. (b) Wasielewski, M. R. *Acc. Chem. Res.* **2009**, *42*, 1910. (c) Lipfert, J.; Doniach, S. *Annu. Rev. Biophys. Biomol. Struct.* **2007**, *36*, 307. (d) Pastor, A.; Martinez-Viviente, E. *Coord. Chem. Rev.* **2008**, *252*, 2314. (e) Petoukhov, M. V.; Svergun, D. I. *Curr. Opin. Struct. Biol.* **2007**, *17*, 562.

(7) (a) Dahneke, B. E. *Measurements of suspended particles by quasi-elastic light scattering*; Wiley: New York, 1983. (b) Pecora, R. *Dynamic light scattering: applications of photon correlation spectroscopy*; Plenum Press: New York, 1985. (c) Kaszuba, M.; McKnight, D.; Connah, M. T.; McNeil-Watson, F. K.; Nobbmann, U. *J. Nanopart. Res.* **2008**, *10*, 823.

(8) (a) Longoni, G.; Chini, P. *J. Am. Chem. Soc.* **1976**, *98*, 7225. (b) Calabrese, J. C.; Dahl, L. F.; Chini, P.; Longoni, G.; Martinengo, S. *J. Am. Chem. Soc.* **1974**, *96*, 2614.

(9) Femoni, C.; Kaswalder, F.; Iapalucci, M. C.; Longoni, G.; Mehlstäubl, M.; Zacchini, S. *Chem. Commun.* **2005**, *46*, 5769.

(10) (a) Femoni, C.; Kaswalder, F.; Iapalucci, M. C.; Longoni, G.; Mehlstäubl, M.; Zacchini, S.; Ceriotti, A. *Angew. Chem., Int. Ed.* **2006**, *45*, 2060. (b) Femoni, C.; Kaswalder, F.; Iapalucci, M. C.; Longoni, G.; Zacchini, S. *Eur. J. Inorg. Chem.* **2007**, 1483.

(11) (a) Greco, P.; Cavallini, M.; Stoliar, P.; Quiroga, S. D.; Dutta, S.; Zacchini, S.; Iapalucci, M. C.; Morandi, V.; Milita, S.; Merli, P. G.; Biscarini, F. *J. Am. Chem. Soc.* **2008**, *130*, 1177. (b) Serban, D. A.; Greco, P.; Melinte, S.; Vlad, A.; Dutu, C. A.; Zacchini, S.; Iapalucci, M. C.; Biscarini, F.; Cavallini, M. *Small* **2009**, *5*, 1117.

Published on Web 06/10/2010

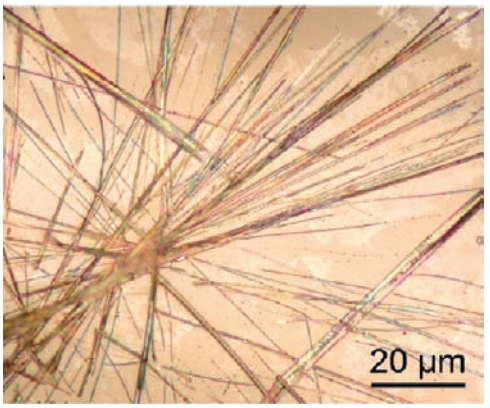

Figure 1. Optical micrographs (magnification 50×) of whisker-like crystals of $[NBu_4]_2[Pt_{15}(CO)_{30}]$. Image reprinted with permission from ref 11a. Copyright 2008 American Chemical Society.

where anions and cations are separated by normal van der Waals contacts and do not show any supramolecular ordering of the anions.[10] Conversely, the highest nuclearity species (n = 5−8) often afford crystals similar to whiskers (see, for instance, Figure 1) as a function of the tetrasubstituted ammonium cation.[10,11] The whiskers contain the self-assembly of aligned chains of cluster anions.

As summarized in Figure 2, continuous, semicontinuous, or discontinuous chains of cluster anions have already been documented.[10] In discontinuous chains, the cluster anions maintain their molecular identity, with the outer $Pt_3(CO)_6$ moieties of consecutive cluster anions being separated by distances slightly above the sum of the van der Waals radii (see Figure 2a). Conversely, continuous chains are characterized by infinite stacks of $Pt_3(CO)_6$ units at bonding distances and, therefore, the molecular identity of the single anion is lost (Figure 2c); the formula of the resulting $[NR_4]_2[Pt_{3n}(CO)_{6n}]$ salt can only be gathered from the number of cations and $Pt_3(CO)_6$ moieties present in the unit cell.

Finally, semicontinuous chains (Figure 2b) display a morphology intermediate between the above two; a $Pt_3(CO)_6$ unit is systematically shared by two contiguous $[Pt_{3(n-1)}(CO)_{6(n-1)}]^{2-}$ anions and displays Pt−Pt interactions intermediate between those of continuous and discontinuous situations. A continuum of situations for the packing of $[Pt_{3n}(CO)_{6n}]^{2-}$ anions is, therefore, possible, and this point will be discussed in detail in the present paper.

Besides, the resulting chains of clusters are usually further organized into 1-D, 2-D, or 3-D packings.[10] The terms 1-D, 2-D, and 3-D are used here in order to distinguish infinite chains arranged along a single direction (parallel chains), two different directions (layered packing), or three noncoplanar directions. Further ordering can also be found. For instance, the parallel chains of cluster anions in 1-D packings often do form hexagonal channels, which lodge the cations.[10] In the case of 2-D packings, the two directions on two consecutive planes can be perfectly orthogonal or form an angle different from 90°, as in the cases previously reported for $[NEt_4]_2[Pt_{24}(CO)_{48}]$ and $[NBu_4]_2[Pt_{24}(CO)_{48}]$, respectively.[10]

As a further point of interest, the self-organized infinite chains morphologically and functionally resemble CO-sheathed platinum wires. In fact, previously reported electrical resistivity measurements on pressed pellets indicated that ionic 0-D materials are electrical insulators, whereas the resistivity drops to ca. 10^5, 10^3, and 10^2 Ω cm upon passing to

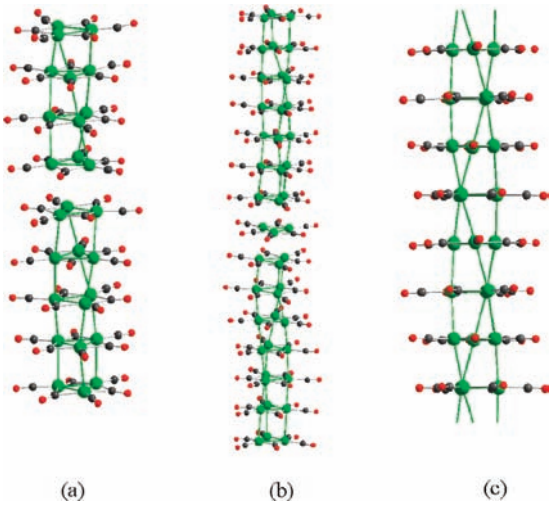

Figure 2. Typical arrangements of $[Pt_{3n}(CO)_{6n}]^{2-}$ (n = 5−8) clusters in (a) discontinuous, (b) semicontinuous, and (c) continuous chains.[10].

discontinuous, semicontinuous, and continuous materials, respectively.[10] This opened the possibility of using the above soluble cluster salts as printable metals in molecular and nanoelectronic structures.[11] It must be remarked that the physical properties of molecular wires based on metal carbonyl clusters have remained unexplored for a long time, and only recently have they been systematically studied by us[10,11] as well as other groups.[12]

Because only two short communications appeared previously on this subject, describing the structures and crystal packing of $[NBu_4]_2[Pt_{12}(CO)_{24}]$, $[NMe_4]_2[Pt_{12}(CO)_{24}]$, $[NEt_4]_2[Pt_{15}(CO)_{30}]$, $[NMe_4]_2[Pt_{18}(CO)_{36}]\cdot 2CH_3COCH_3$, $[NEt_4]_2[Pt_{24}(CO)_{48}]$, and $[NBu_4]_2[Pt_{24}(CO)_{48}]$,[10] herein we report a comprehensive study discussing the different parameters that influence the self-assembly of $[Pt_{3n}(CO)_{6n}]^{2-}$ (n = 4−8) clusters into 0-D, 1-D, 2-D, and 3-D materials as well as their electrical properties. Previously reported $[NR_4]_2[Pt_{3n}(CO)_{6n}]$ salts[10] are therefore included in the discussion of the newly prepared salts of the same clusters with divalent cations such as $[Ru(tpy)_2]^{2+}$ (tpy = 2,2′:6′,2″-terpyridine), $[Ru(bpy)_3]^{2+}$ (bpy = 2,2′-bipyridyl), and $[Ni(macro)]^{2+}$ (macro = 5,7,7,12,14,14-hexamethyl-1,4,8,11-tetraaza-4,11-cyclotetradecadiene). Preliminary results of possible self-assembly phenomena in a solution of $[Pt_{15}(CO)_{30}]^{2-}$ and $[Pt_{18}(CO)_{36}]^{2-}$ according to DLS experiments are also reported.

Experimental Section

General Procedures. All reactions and sample manipulations were carried out using standard Schlenk techniques under nitrogen and in dried solvents. All of the reagents were commercial products (Aldrich) of the highest purity available and were used as received. The $Na_2[Pt_{3n}(CO)_{6n}]$ (n = 3−7),[8] $[Ru(tpy)_2]Cl_2$,[13] $[Ru(bpy)_3][PF_6]_2$,[14] $[Ru(bpy)_2(2\text{-PTZ})][PF_6]$,[15] and $[Ni(macro)][BF_4]_2$[16] salts have been prepared according to the literature.

(12) (a) Shieh, M.; Ho, C.-H.; Sheu, W.-S.; Chen, B.-G.; Chu, Y.-Y.; Miu, C.-Y.; Liu, H.-L.; Shen, C.-C. *J. Am. Chem. Soc.* **2008**, *130*, 14114. (b) Shieh, M.; Hsu, M.-H.; Sheu, W.-S.; Jang, L.-F.; Lin, S.-F.; Chu, Y.-Y.; Miu, C.-Y.; Lai, Y.-W.; Liu, H.-L.; Her, J. L. *Chem.—Eur. J.* **2007**, *13*, 6605.
(13) Braddock, J. N.; Meyer, T. J. *J. Am. Chem. Soc.* **1973**, *95*, 3158.
(14) Caspar, J. V.; Meyer, T. J. *J. Am. Chem. Soc.* **1983**, *105*, 5583.
(15) Stagni, S.; Orselli, E.; Palazzi, A.; De Cola, L.; Zacchini, S.; Femoni, C.; Marcaccio., M.; Paolucci, F.; Zanarini, S. *Inorg. Chem.* **2007**, *46*, 9126.
(16) (a) Furenlid, L. R.; Renner, M. W.; Szalda, D. J.; Fujita, E. *J. Am. Chem. Soc.* **1991**, *113*, 883. (b) Bailey, M. F.; Maxwell, I. E. *Chem. Commun.* **1966**, 908.

Analyses of platinum, ruthenium, and nickel were performed by atomic absorption on a Pye-Unicam instrument. Analyses of carbon, hydrogn, and nickel were obtained with a ThermoQuest FlashEA 1112NC instrument. IR spectra were recorded on a Perkin-Elmer SpectrumOne interferometer in CaF_2 cells. Electrical resistivity measurements have been carried out under nitrogen in a glovebag with a Keithley 2400 SourceMeter on polycrystalline materials pressed into pellets (diameter 8 or 13 mm, thickness ca. 1 mm) using the four-point method. Structure drawings have been performed with *SCHAKAL99*[17] and *Diamond*.[18]

Synthesis of $[Ru(tpy)_2][Pt_{12}(CO)_{24}]\cdot 4CH_3COCH_3$. $[Ru(tpy)_2]Cl_2$ (0.382 g, 0.598 mmol) dissolved in methanol (15 mL) was slowly added to a methanol solution (20 mL) of $Na_2[Pt_{12}(CO)_{24}]$ (1.22 g, 0.399 mmol), resulting in the partial precipitation of $[Ru(tpy)_2][Pt_{12}(CO)_{24}]$. Complete precipitation was then accomplished by adding water (20 mL). The solid was recovered by filtration, washed with water (20 mL) and tetrahydrofuran (THF; 20 mL), and extracted in acetone (15 mL). Crystals of $[Ru(tpy)_2][Pt_{12}(CO)_{24}]\cdot 4CH_3COCH_3$ were grown by layering isopropyl alcohol (30 mL) on the acetone solution (yield 1.16 g, 76%).

Elem. anal. Calcd for $C_{66}H_{46}N_6O_{28}Pt_{12}Ru$ (3813.24): C, 20.79; H, 1.22; N, 2.20; Ru, 2.65; Pt, 61.39. Found: C, 20.95; H, 1.04; N, 2.01; Ru, 2.84; Pt, 61.52. IR (acetone, 293 K): ν(CO) 2047(vs), 1865(m) cm^{-1}.

Synthesis of $[Ni(macro)][Pt_{12}(CO)_{24}]\cdot 2CH_3COCH_3$. $[Ni(macro)][BF_4]_2$ (0.158 g, 0.564 mmol) dissolved in methanol (15 mL) was slowly added to a methanol solution (20 mL) of $Na_2[Pt_{12}(CO)_{24}]$ (1.15 g, 0.376 mmol), resulting in the partial precipitation of $[Ni(macro)][Pt_{12}(CO)_{24}]$. Complete precipitation was then accomplished by adding water (20 mL). The solid was recovered by filtration, washed with water (20 mL) and THF (20 mL), and extracted in acetone (15 mL). Crystals of $[Ni(macro)][Pt_{12}(CO)_{24}]\cdot 2CH_3COCH_3$ were grown by layering isopropyl alcohol (30 mL) on the acetone solution (yield 0.94 g, 72%).

Elem. anal. Calcd for $C_{46}H_{44}N_4NiO_{26}Pt_{12}$ (3468.48): C, 15.93; H, 1.28; N, 1.62; Ni, 1.69; Pt, 67.49. Found: C, 16.08; H, 1.44; N, 1.51; Ni, 1.49; Pt, 67.58. IR (acetone, 293 K): ν(CO) 2047(vs), 1865(m) cm^{-1}.

Synthesis of $[Ru(tpy)_2][Pt_{15}(CO)_{30}]\cdot 3DMF$. $[Ru(tpy)_2]Cl_2$ (0.257 g, 0.598 mmol) dissolved in methanol (15 mL) was slowly added to a methanol solution (20 mL) of $Na_2[Pt_{15}(CO)_{30}]$ (1.02 g, 0.268 mmol), resulting in the partial precipitation of $[Ru(tpy)_2][Pt_{15}(CO)_{30}]$. Complete precipitation was then accomplished by adding water (20 mL). The solid was recovered by filtration, washed with water (20 mL), THF (20 mL), and acetone (20 mL), and extracted in *N*,*N*-dimethylformamide (DMF; 15 mL). Crystals of $[Ru(tpy)_2][Pt_{15}(CO)_{30}]\cdot 3DMF$ were obtained by layering isopropyl alcohol (30 mL) on the DMF solution (yield 0.95 g, 78%).

Elem. anal. Calcd for $C_{69}H_{43}N_9O_{33}Pt_{15}Ru$ (4553.36): C, 18.20; H, 0.95; N, 2.77; Ru, 2.22; Pt, 64.26. Found: C, 18.48; H, 0.78; N, 2.95; Ru, 2.41; Pt, 64.44. IR (DMF, 293 K): ν(CO) 2054(vs), 1873(m) cm^{-1}.

Synthesis of $[Ru(bpy)_3][Pt_{15}(CO)_{30}]\cdot 3CH_3COCH_3$. $[Ru(bpy)_3][PF_6]_2$ (0.699 g, 0.813 mmol) dissolved in methanol (15 mL) was slowly added to a methanol solution (20 mL) of $Na_2[Pt_9(CO)_{18}]$ (1.25 g, 0.542 mmol), resulting in the partial precipitation of $[Ru(bpy)_3][Pt_9(CO)_{18}]$. Complete precipitation was then accomplished by adding water (20 mL). The solid was recovered by filtration, washed with water (20 mL) and THF (20 mL), and extracted in acetone (15 mL). Isopropyl alcohol (30 mL), containing a few crystals of I_2 (used for oxidizing $[Pt_9(CO)_{18}]^{2-}$ to $[Pt_{15}(CO)_{30}]^{2-}$), was layered on the acetone solution, resulting in a complex mixture of products, from which a few crystals of $[Ru(bpy)_3][Pt_{15}(CO)_{30}]\cdot 3CH_3COCH_3$ suitable for X-ray analysis were mechanically separated.

Synthesis of $[Ru(bpy)_3][Pt_{18}(CO)_{36}]$. $[Ru(bpy)_3][PF_6]_2$ (0.418 g, 0.486 mmol) dissolved in methanol (15 mL) was slowly added to a methanol solution (20 mL) of $Na_2[Pt_{18}(CO)_{36}]$ (1.48 g, 0.324 mmol), resulting in the partial precipitation of $[Ru(bpy)_3][Pt_{18}(CO)_{36}]$. Complete precipitation was then accomplished by adding water (20 mL). The solid was recovered by filtration, washed with water (20 mL), THF (20 mL), and acetone (20 mL), and extracted in DMF (15 mL). Crystals of $[Ru(bpy)_3][Pt_{18}(CO)_{36}]$ were obtained by layering isopropyl alcohol (30 mL) on the DMF solution (yield 1.12 g, 68%).

Elem. anal. Calcd for $C_{66}H_{24}N_6O_{36}Pt_{18}Ru$ (5089.39): C, 15.58; H, 0.48; N, 1.65; Ru, 1.99; Pt, 68.99. Found: C, 15.35; H, 0.54; N, 1.37; Ru, 2.08; Pt, 68.81. IR (DMF, 293 K): ν(CO) 2063(vs), 1879(m) cm^{-1}.

Synthesis of $[Ru(bpy)_2(2\text{-}PTZ)]_2[Pt_{18}(CO)_{36}]$. $[Ru(bpy)_2(2\text{-}PTZ)][PF_6]$ (0.788 g, 1.12 mmol) dissolved in methanol (15 mL) was slowly added to a methanol solution (20 mL) of $Na_2[Pt_{12}(CO)_{24}]$ (1.14 g, 0.373 mmol), resulting in the partial precipitation of $[Ru(bpy)_2(2\text{-}PTZ)]_2[Pt_{12}(CO)_{24}]$. Complete precipitation was then accomplished by adding water (20 mL). The solid was recovered by filtration, washed with water (20 mL) and THF (20 mL), and extracted in acetone (15 mL). Isopropyl alcohol (30 mL), containing a few crystals of I_2 (used for oxidizing $[Pt_{12}(CO)_{24}]^{2-}$ to $[Pt_{18}(CO)_{36}]^{2-}$), was layered on the acetone solution, resulting in a complex mixture of products, from which a few crystals of $[Ru(bpy)_2(2\text{-}PTZ)]_2[Pt_{18}(CO)_{36}]$ suitable for X-ray analysis were mechanically separated.

Synthesis of $[Ru(tpy)_2][Pt_{21}(CO)_{42}]\cdot 2DMF$. $[Ru(tpy)_2]Cl_2$ (0.166 g, 0.386 mmol) dissolved in methanol (15 mL) was slowly added to a methanol solution (20 mL) of $Na_2[Pt_{21}(CO)_{42}]$ (1.37 g, 0.258 mmol), resulting in the partial precipitation of $[Ru(tpy)_2][Pt_{21}(CO)_{42}]$. Complete precipitation was then accomplished by adding water (20 mL). The solid was recovered by filtration, washed with water (20 mL), THF (20 mL), and acetone (20 mL), and extracted in DMF (15 mL). Crystals of $[Ru(tpy)_2][Pt_{21}(CO)_{42}]\cdot 2DMF$ were obtained by layering isopropyl alcohol (30 mL) on the DMF solution (yield 1.05 g, 68%).

Elem. anal. Calcd for $C_{78}H_{36}N_8O_{44}Pt_{21}Ru$ (5986.86): C, 15.65; H, 0.61; N, 1.87; Ru, 1.69; Pt, 68.43. Found: C, 15.77; H, 0.75; N, 1.69; Ru, 1.52; Pt, 68.59. IR (DMF, 293 K): ν(CO) 2068(vs), 1881(m) cm^{-1}.

X-ray Crystallographic Studies. Crystal data and collection details for $[Ru(tpy)_2][Pt_{12}(CO)_{24}]\cdot 4CH_3COCH_3$, $[Ni(macro)][Pt_{12}(CO)_{24}]\cdot 2CH_3COCH_3$, $[Ru(tpy)_2][Pt_{15}(CO)_{30}]\cdot 3DMF$, $[Ru(bpy)_3][Pt_{15}(CO)_{30}]\cdot 3CH_3COCH_3$, $[Ru(bpy)_3][Pt_{18}(CO)_{36}]$, $[Ru(bpy)_2(2\text{-}PTZ)]_2[Pt_{18}(CO)_{36}]$, and $[Ru(tpy)_2][Pt_{21}(CO)_{42}]\cdot 2DMF$ are reported in Table 1. The diffraction experiments were carried out on a Bruker APEX II diffractometer equipped with a CCD detector using Mo Kα radiation. Data were corrected for Lorentz polarization and absorption effects (empirical absorption correction *SADABS*).[19] Structures were solved by direct methods and refined by full-matrix least squares based on all data using F^2.[20] Hydrogen atoms were fixed at calculated positions and refined by a riding model. All non-hydrogen atoms were refined with anisotropic displacement parameters, unless otherwise stated. Solution and refinement of all of these structures presented several difficulties because of the fact that diffraction is mainly dominated by the periodical arrangement of the triangular platinum units, which are sometimes disordered. The treatment of lighter atoms, in particular cocrystallized solvent molecules, required the introduction of several restraints in order to reach convergence. As discussed below, some noncompletely resolved

(17) Keller, E. *SCHAKAL99*; University of Freiburg: Freiburg, Germany, 1999.

(18) *DIAMOND—Visual Crystal Structure Information System*; Crystal Impact: Bonn, Germany.

(19) Sheldrick, G. M. *SADABS, Program for empirical absorption correction*; University of Göttingen: Göttingen, Germany, 1996.

(20) Sheldrick, G. M. *SHELX97, Program for crystal structure determination*; University of Göttingen: Göttingen, Germany, 1997.

Table 1. Crystal Data and Experimental Details for $[Ru(tpy)_2][Pt_{12}(CO)_{24}]\cdot 4CH_3COCH_3$, $[Ni(macro)][Pt_{12}(CO)_{24}]\cdot 2CH_3COCH_3$, $[Ru(tpy)_2][Pt_{15}(CO)_{30}]\cdot 3DMF$, $[Ru(bipy)_3][Pt_{15}(CO)_{30}]\cdot 3CH_3COCH_3$, $[Ru(bipy)_3][Pt_{18}(CO)_{36}]$, $[Ru(bipy)_2(L\text{-}L)]_2[Pt_{18}(CO)_{36}]$, and $[Ru(tpy)_2][Pt_{21}(CO)_{42}]\cdot 2DMF$

	$[Ru(tpy)_2][Pt_{12}(CO)_{24}]\cdot 4CH_3COCH_3$	$[Ni(macro)][Pt_{12}(CO)_{24}]\cdot 2CH_3COCH_3$	$[Ru(tpy)_2][Pt_{15}(CO)_{30}]\cdot 3DMF$	$[Ru(bpy)_3][Pt_{15}(CO)_{30}]\cdot 3CH_3COCH_3$	$[Ru(bpy)_3][Pt_{18}(CO)_{36}]$	$[Ru(bpy)_2(2\text{-}PTZ)]_2[Pt_{18}(CO)_{36}]$	$[Ru(tpy)_2][Pt_{21}(CO)_{42}]\cdot 2DMF$
formula	$C_{66}H_{46}N_6O_{28}Pt_{12}Ru$	$C_{46}H_{44}N_4NiO_{26}Pt_{12}$	$C_{69}H_{43}N_9O_{33}Pt_{15}Ru$	$C_{69}H_{42}N_6O_{33}Pt_{15}Ru$	$C_{66}H_{24}N_6O_{36}Pt_{18}Ru$	$C_{88}H_{40}N_{18}O_{36}Pt_{18}Ru_2$	$C_{78}H_{36}N_8O_{44}Pt_{21}Ru$
fw	3813.24	3468.64	4553.39	4510.51	5089.60	5639.14	5987.11
T, K	294(2)	294(2)	100(2)	293(2)	294(2)	293(2)	100(2)
λ, Å	0.710 73	0.710 73	0.710 73	0.710 73	0.710 73	0.710 73	0.710 73
cryst syst	monoclinic	triclinic	triclinic	hexagonal	monoclinic	monoclinic	triclinic
space group	$P2_1/n$	$P\bar{1}$	$P\bar{1}$	$P6_3$	$P2_1/c$	$C2/m$	$P\bar{1}$
a, Å	15.3425(17)	12.6213(175)	15.785(2)	18.0804(9)	18.827(3)	37.690(4)	16.511(5)
b, Å	19.052(2)	16.750(2)	18.572(3)	18.0804(9)	29.294(5)	9.3606(2)	18.832(5)
c, Å	28.302(3)	17.948(2)	18.910(3)	16.0241(11)	18.596(3)	20.488(2)	21.372(6)
α, deg	90	87.098(2)	102.284(2)	90	90	90	105.080(4)
β, deg	92.898(2)	71.932(2)	104.012(2)(10)	90	109.232(2)	121.5300(10)	106.354(4)
γ, deg	90	70.122(2)	111.170(2)	120	90	90	109.421(4)
cell volume, Å^3	8262.1(16)	3385.9(7)	4731.6(12)	4536.5(4)	9684(3)	6161.1(10)	5535(3)
Z	4	2	2	2	4	2	2
D_c, g cm^{-3}	3.066	3.402	3.196	3.302	3.491	3.040	3.592
μ, mm^{-1}	20.482	25.024	22.306	23.262	26.110	20.653	26.629
F(000)	6752	3040	3996	3952	8792	4948	5188
cryst size, mm	0.19 × 0.13 × 0.11	0.15 × 0.12 × 0.10	0.15 × 0.12 × 0.11	0.16 × 0.12 × 0.11	0.13 × 0.10 × 0.09	0.14 × 0.11 × 0.10	0.14 × 0.11 × 0.10
θ limits, deg	1.29−25.68	1.20−25.03	1.18−25.03	1.30−25.03	1.34−25.03	1.99−25.03	1.25−25.03
index ranges	$-18 \le h \le 18$ $-23 \le k \le 23$ $-34 \le l \le 34$	$-15 \le h \le 15$ $-19 \le k \le 19$ $-21 \le l \le 21$	$-18 \le h \le 18$ $-22 \le k \le 22$ $-22 \le l \le 22$	$-21 \le h \le 21$ $-21 \le k \le 21$ $-19 \le l \le 19$	$-22 \le h \le 22$ $-34 \le k \le 34$ $-22 \le l \le 22$	$-44 \le h \le 44$ $-11 \le k \le 11$ $-24 \le l \le 24$	$-19 \le h \le 19$ $-22 \le k \le 22$ $-25 \le l \le 25$
reflns collected	76 106	32 317	44 812	33 021	89 752	29 212	50 333
indep reflns	15 665 [R_{int} = 0.0842]	11 906 [R_{int} = 0.0428]	16 664 [R_{int} = 0.0778]	5346 [R_{int} = 0.1198]	16 973 [R_{int} = 0.1150]	5743 [R_{int} = 0.0844]	19 483 [R_{int} = 0.0776]
completeness to θ = 25.03°, %	99.9	99.6	99.7	100.0	99.2	99.1	99.5
data/restraints/parameters	15 665/527/938	11 906/905/802	16 664/865/1210	5346/191/374	16 973/1020/1172	5743/673/448	19 483/885/1526
GOF on F^2	1.001	1.017	1.333	1.002	1.030	1.078	1.005
R1 [$I > 2\sigma(I)$]	0.0711	0.0388	0.0794	0.0508	0.0802	0.0741	0.0554
wR2 (all data)	0.2616	0.1005	0.2283	0.0994	0.2425	0.1784	0.1656
largest diff. peak and hole, e Å^{-3}	3.689/−4.047	1.252/−1.656	3.716/−3.392	1.105/−1.491	5.945/−4.415	2.759/−2.605	4.241/−5.077

problems remained (usually ALERT B and C of *PLATON*),[21] but in view of the complexity of the structures and of the fact that the main structural features are comparable and similar in all of the crystals examined as well as in previously reported structures for analogous systems with different cations, it can be concluded that the proposed models are completely reliable.

$[Ru(tpy)_2][Pt_{12}(CO)_{24}]\cdot 4CH_3COCH_3$. The asymmetric unit contains the cluster anion, one cation, and four acetone molecules all located in general positions. Similar *U* restraints were applied to the carbon and oxygen atoms (s.u. 0.01). The four independent acetone molecules have been treated isotropically by applying similar geometrical restraints (SAME instruction in *SHELXL*). Restraints to bond distances were applied as follows: 1.51 Å (s.u. 0.01) for C−C and 1.21 Å (s.u. 0.01) for C═O in acetone. Some high residual electron densities remain especially close to platinum atoms after the final refinement, probably because of the low quality of these platelike crystals.

[Ni(macro)]$[Pt_{12}(CO)_{24}]\cdot 2CH_3COCH_3$. The asymmetric unit contains the cluster anion, one cation, and two acetone molecules all located in general positions. Similar *U* restraints were applied to the carbon and oxygen atoms (s.u. 0.003). The thermal ellipsoids of the carbonyl ligands were restrained to an isotropic-like behavior (ISOR line in *SHELXL*; s.u. 0.005). Rigid bond restraints were applied to the cluster anion (s.u. 0.01). Restraints to bond distances were applied as follows: 1.51 Å (s.u. 0.01) for C−C and 1.21 Å (s.u. 0.01) for C═O in acetone.

$[Ru(tpy)_2][Pt_{15}(CO)_{30}]\cdot 3DMF$. The asymmetric unit contains the cluster anion, one cation, and three DMF molecules all located in general positions. The cluster anion displays extended disorder, and in order to try to account for it, the following model has been adopted: the three triangular units comprising (I) Pt(1)−Pt(2)−Pt(3), (II) Pt(4)−Pt(5)−Pt(6), and (III) Pt(7)−Pt(8)−Pt(9) were split into two positions each and refined anisotropically using one occupancy parameter per disordered group. In the case of units I and II, only the platinum atoms have been split, whereas for III, also the relative six CO ligands have been included in the disorder model. The three independent occupancy factors refined as (I) 0.513(3), (II) 0.522(3), and (III) 0.5931(13). Also, one of the three DMF molecules is disordered over two positions and, therefore, it has been consequently split and refined using one independent occupancy factor. All three DMF molecules have been refined isotropically. Similar *U* restraints were applied to the carbon, oxygen, nitrogen, and platinum atoms (s.u. 0.001). The aromatic atoms of the $[Ru(tpy)]^{2+}$ cation have been constrained to perfect hexagons (AFIX 66 line in *SHELXL*). Restraints to bond distances were applied as follows (s.u. 0.01): 1.83 Å for $Pt-C_{terminal}$, 2.01 Å for $Pt-C_{bridging}$, 1.15 Å for $C-O_{terminal}$, and 1.18 Å for $C-O_{bridging}$ in the disordered unit III; 1.21 Å for C═O, 1.37 Å for $C(sp^2)-N$, and 1.46 Å for $C(sp^3)-N$ in DMF. A large solvent/anion *C* U_{eq}(max)/U_{eq}(min) (10.00 ratio) remains in the final refinement probably because it has not been possible to completely account for the whole disorder of the DMF molecules. Several crystals have been examined, always giving very similar results.

$[Ru(bpy)_3][Pt_{15}(CO)_{30}]\cdot 3CH_3COCH_3$. The asymmetric unit contains one-third of the cluster anion, one-third of the cation, and one independent acetone molecule. The complete anion and cation have been obtained by applying the 6_3 axis, resulting in two $[Ru(bpy)_3][Pt_{15}(CO)_{30}]\cdot 3CH_3COCH_3$ unit formulas per unit cell ($Z = 2$). The crystals are racemically twinned with a refined Flack parameter of 0.09(2),[22] and it was, therefore, refined using the TWIN refinement routine of *SHELXTL*. Similar *U* restraints were applied to the carbon, oxygen, and platinum atoms (s.u. 0.003). Rigid bond restraints were applied to the cluster anion (s.u. 0.003).

$[Ru(bpy)_3][Pt_{18}(CO)_{36}]$. The asymmetric unit contains the cluster anion and one cation all located in general positions. The cluster anion displays partial disorder, and in particular the unit comprising Pt(7)−Pt(8)−Pt(9) was split into two positions and refined anisotropically using one occupancy parameter per disordered group. Similar *U* restraints were applied to the carbon, oxygen, and nitrogen atoms (s.u. 0.01). Rigid bond restraints were applied to the cluster anion and the cation (s.u. 0.005). Restraints to bond distances were applied as follows (s.u. 0.01): 1.15 Å for C−O in the whole cluster anion. The crystal is likely to contain some highly disordered DMF molecules (residual void in the unit cell 169.00 $Å^3$), but it has not been possible to locate and refine them because of the low quality of the crystals. The compound, in fact, crystallizes under all experimental conditions, resulting in very small needles.

$[Ru(bpy)_2(2\text{-}PTZ)]_2[Pt_{18}(CO)_{36}]$. The asymmetric unit contains one-third of the cluster anion and half of a cation. By application to the independent part of the cluster anion, the *m* plane half of the cluster is generated; the whole molecule is then obtained by packing together two unit cells. The cation is disordered over four symmetry-related positions, and it has been refined with occupancy factor 10.5 in order to satisfy the molecular formula. Because of the heavy disorder of the cation, it has been treated as a rigid group using the crystallographic coordinates imported from another crystal structure of the $[Ru(bpy)_2(2\text{-}PTZ)]^+$ cation (FRAG and FEND lines in *SHELXL* with an appropriate AFIX line). The unit cell probably contains a few disordered molecules of solvent (residual void in the unit cell 158.00 $Å^3$), but the above-mentioned disorder as well as the presence of several heavy atoms hampered their location. Restraints to bond distances were applied as follows (s.u. 0.01): 1.15 Å for C−O in the whole cluster anion.

$[Ru(tpy)_2][Pt_{21}(CO)_{42}]\cdot 2DMF$. The asymmetric unit contains the cluster anion, one cation, and two DMF molecules, all located in general positions. The cluster anion displays extended disorder, and in order to try to account for it, the following model has been adopted: the two triangular units comprising (I) Pt(1)−Pt(2)−Pt(3) and (II) Pt(19)−Pt(20)−Pt(21) were split into two positions each and refined anisotropically using one occupancy parameter per disordered group. In the case of unit I, only the platinum atoms have been split, whereas for II, also the six relative CO ligands have been included in the disorder model. The two independent occupancy factors were refined as (I) 0.9573(11) and (II) 0.5289(13). Also, one of the two DMF molecules is disordered over three positions and, therefore, it has been, consequently, split and refined using three independent occupancy factors, whose sum was restrained to the unit. All DMF molecules have been refined isotropically. Similar *U* restraints were applied to the carbon, oxygen, nitrogen, and platinum atoms (s.u. 0.003). Restraints to bond distances were applied as follows (s.u. 0.01): 1.83 Å for $Pt-C_{terminal}$, 2.01 Å for $Pt-C_{bridging}$, 1.15 Å for $C-O_{terminal}$, and 1.18 Å for $C-O_{bridging}$ in the disordered unit II; 1.21 Å for C═O, 1.37 Å for $C(sp^2)-N$, and 1.46 Å for $C(sp^3)-N$ in DMF. Because of the disorder, some short contacts, mainly involving the DMF molecules and/or CO ligands, remain.

DLS Measurements. DLS measurements have been carried out on a Malvern Zetasizer Nano S (Malvern Instruments Ltd., Worcestershire, U.K.) with a detection angle of 173°. All measurements in this study were taken at temperatures of 20 and 2 °C. At least four repeat measurements on each sample were taken to check for the resulting repeatability. The Nano S uses a 4 mW He−Ne laser operating at a wavelength of 633 nm. The intensity size distributions were obtained from analysis of the correlation functions using the Multiple Narrow Modes algorithm in the instrument software.[23] Samples were prepared

(21) Spek, A. L. *PLATON, A Multipurpose Crystallographic Tool*; Utrecht University: Utrecht, The Netherlands, 2005.

(22) Flack, H. D. *Acta Crystallogr., Sect. A* **1983**, *39*, 876.

(23) (a) Twomey, S. *Introduction to the mathematics of inversion of remote sensing and indirect measurements*; Dover Publication: New York, 1997. (b) Lawson, C. L.; Hanson, R. J. *Solving least squares problems*; Society for Industrial and Applied Mathematics (SIAM): Philadelphia, PA, 1995.

under nitrogen by dissolving $[NBu_4]_2[Pt_{15}(CO)_{30}]$ or $[NBu_4]_2[Pt_{18}(CO)_{36}]$ in acetonitrile in order to have a 0.2 wt % solution, and this was then filtered through Whatman Anotop 0.20, 0.10, or 0.02 μm pore size filters.

Results and Discussion

1. Synthesis. The $[Pt_{3n}(CO)_{6n}]^{2-}$ ($n = 4-7$) anions have been prepared by the controlled reduction of $Na_2[Pt_{30}(CO)_{60}]$ in CH_3OH with NaOH under a CO atmosphere according to the literature.[8] The formal stoichiometry for the formation of $[Pt_{15}(CO)_{30}]^{2-}$ is reported in eq 1, as an example.

$$[Pt_{30}(CO)_{60}]^{2-} + CO + 3OH^- \rightarrow 2[Pt_{15}(CO)_{30}]^{2-} + HCO_3^- + H_2O \quad (1)$$

The resulting $Na_2[Pt_{3n}(CO)_{6n}]$ ($n = 4-7$) sodium salts are very soluble in methanol, and complete metathesis of the cation has successfully been performed by the addition of a methanolic solution of $[Ru(tpy)_2]Cl_2$, $[Ru(bpy)_3][PF_6]_2$, $[Ru(bpy)_2(2\text{-PTZ})][PF_6]$ [2-PTZ = 5-(2-piridyl)-tetrazolate], or $[Ni(macro)][BF_4]_2$ salts, respectively. Precipitation has been completed by the addition of water. As expected, the $[Ru(tpy)_2]^{2+}$, $[Ru(bpy)_3]^{2+}$, and $[Ni(macro)]^{2+}$ salts of the $[Pt_{3n}(CO)_{6n}]^{2-}$ anions are less soluble than their corresponding $[NR_4]^+$ salts. Thus, the $[NR_4]_2[Pt_{3n}(CO)_{6n}]$ salts with $n \leq 5$ are usually soluble in organic solvents such as THF, acetone, and acetonirile. Their solubility only progressively drops for $n \geq 6$.[8-10] In contrast, the corresponding salts with $n = 5-7$ of the investigated divalent cations are only soluble in more polar solvents such as DMF and dimethyl sulfoxide. Thus, while $[Ru(tpy)_2][Pt_{12}(CO)_{24}]\cdot 4CH_3COCH_3$ and $[Ni(macro)][Pt_{12}(CO)_{24}]\cdot 2CH_3COCH_3$ have been successfully crystallized by layering isopropyl alcohol on their acetone solutions, $[Ru(tpy)_2][Pt_{15}(CO)_{30}]\cdot 3DMF$, $[Ru(bpy)_3][Pt_{18}(CO)_{36}]$, and $[Ru(tpy)_2][Pt_{21}(CO)_{42}]\cdot 2DMF$ have been crystallized from DMF/isopropyl alcohol mixtures. Conversely, well-shaped crystals of $[Ru(bpy)_3][Pt_{15}(CO)_{30}]\cdot 3CH_3COCH_3$ and $[Ru(bpy)_2(2\text{-PTZ})]_2[Pt_{18}(CO)_{36}]$ could only be grown by layering isopropyl alcohol on top of acetone solutions of more reduced clusters, such as $[Ru(bpy)_3][Pt_9(CO)_{18}]$ and $[Ru(bpy)_2(2\text{-PTZ})]_2[Pt_{12}(CO)_{24}]$, in the presence of a stoichiometric amount of an oxidizing agent such as $SbCl_3$ or I_2. As a consequence, these two salts have always been obtained in a mixture with the starting materials and have been mechanically separated on the basis of their different morphologies.

The nature and purity of all samples have been established by elemental analysis and IR spectroscopy, and the best shaped crystals have been investigated by single-crystal X-ray diffraction analysis.

2. Description of the Crystal Structures. The crystal structures of the $[Ru(tpy)_2]$ $[Pt_{12}(CO)_{24}]\cdot 4CH_3COCH_3$, $[Ni(macro)][Pt_{12}(CO)_{24}]\cdot 2CH_3COCH_3$, $[Ru(tpy)_2][Pt_{15}(CO)_{30}]\cdot 3DMF$, $[Ru(bpy)_3][Pt_{15}(CO)_{30}]\cdot 3CH_3COCH_3$, $[Ru(bpy)_3][Pt_{18}(CO)_{36}]$, $[Ru(bpy)_2(2\text{-PTZ})]_2[Pt_{18}(CO)_{36}]$, and $[Ru(tpy)_2][Pt_{21}(CO)_{42}]\cdot 2DMF$ salts, which contain $[Pt_{3n}(CO)_{6n}]^{2-}$ ($n = 4-7$) cluster anions, are briefly described by mainly focusing on their crystal packing and stacking of the cluster anions. Some of these anions display crystallographic disorder, mainly due to partial rotation of the $Pt_3(CO)_3(\mu\text{-}CO)_3$ units around the common C_3 axis and, to a minor extent, translation along the same axis. For the sake of simplicity, only the main images of the anions will be considered in the following discussion. Further details on the disorder models adopted in each case are reported in the Experimental Section. The molecular structures of all cations contained in these salts are collected in Figure 3, whereas the cluster dianions and their stacking are shown in Figure 4. The complete crystal packings are reported in Figure 5. Pt−Pt contacts in the $[Pt_{3n}(CO)_{6n}]^{2-}$ ($n = 4-7$) anions are very spread, ranging from covalent interactions to sub van der Waals contacts. Thus, in drawing Figures 4 and 5, it has been arbitrarily decided to represent Pt−Pt bonds up to 3.34 Å, which is slightly below twice the van der Waals radius of platinum and ca. 20% greater than twice its covalent radius.[24] Relevant bonding parameters for these crystal structures are listed in Table 2.

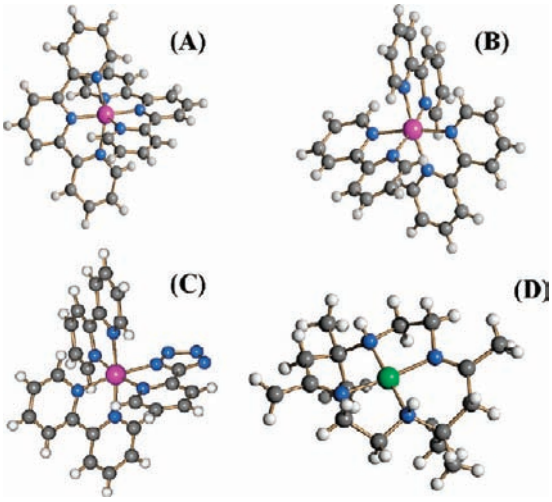

Figure 3. Molecular structures of the cations (A) $[Ru(tpy)_2]^{2+}$, (B) $[Ru(bpy)_3]^{2+}$, (C) $[Ru(bpy)_2(2\text{-PTZ})]^+$, and (D) $[Ni(macro)]^{2+}$.

$[Pt_{12}(CO)_{24}]^{2-}$. Both $[Ru(tpy)_2][Pt_{12}(CO)_{24}]\cdot 4CH_3COCH_3$ and $[Ni(macro)][Pt_{12}(CO)_{24}]\cdot 2CH_3COCH_3$ salts contain the $[Pt_{12}(CO)_{24}]^{2-}$ anion, displaying usual Pt−Pt intratriangular and intertriangular bonding distances (Table 2).[8,9] In this regard, it is worth mentioning that accepted values for the covalent and van der Waals radii of platinum are 1.36 and 1.72 Å, respectively.[24] The distances between the centroids of the $Pt_3(\mu\text{-}CO)_3(CO)_3$ units of $[Pt_{12}(CO)_{24}]^{2-}$ are in the range 3.01−3.06 Å.

The crystal packings of the $[Ru(tpy)_2][Pt_{12}(CO)_{24}]\cdot 4CH_3COCH_3$ and $[Ni(macro)][Pt_{12}(CO)_{24}]\cdot 2CH_3COCH_3$ salts (Figures 4A,B and 5A,B) are typically ionic without any stacking of molecular clusters (0-D packing).

$[Pt_{15}(CO)_{30}]^{2-}$. The $[Ru(tpy)_2][Pt_{15}(CO)_{30}]\cdot 3DMF$ salt is composed of discrete $[Pt_{15}(CO)_{30}]^{2-}$ anions that are stacked into infinite discontinuous chains of clusters (Figure 4C). The gap (distance between the centroids) of two consecutive $[Pt_{15}(CO)_{30}]^{2-}$ units is 3.58 Å. This structure is reminiscent of $[NEt_4]_2[Pt_{15}(CO)_{30}]$[10b] in which the discontinuous chains of $[Pt_{15}(CO)_{30}]^{2-}$ clusters [gap 3.45−3.53 Å] were arranged into a cubic 3-D network. In contrast, the discontinuous

(24) (a) Cordero, B.; Gómez, V.; Platero-Prats, A. E.; Revés, M.; Echevarría, J.; Cremades, E.; Barragán, F.; Alvarez, S. *Dalton Trans.* **2008**, 2832. (b) Bondi, A. *J. Phys. Chem.* **1964**, *68*, 441.

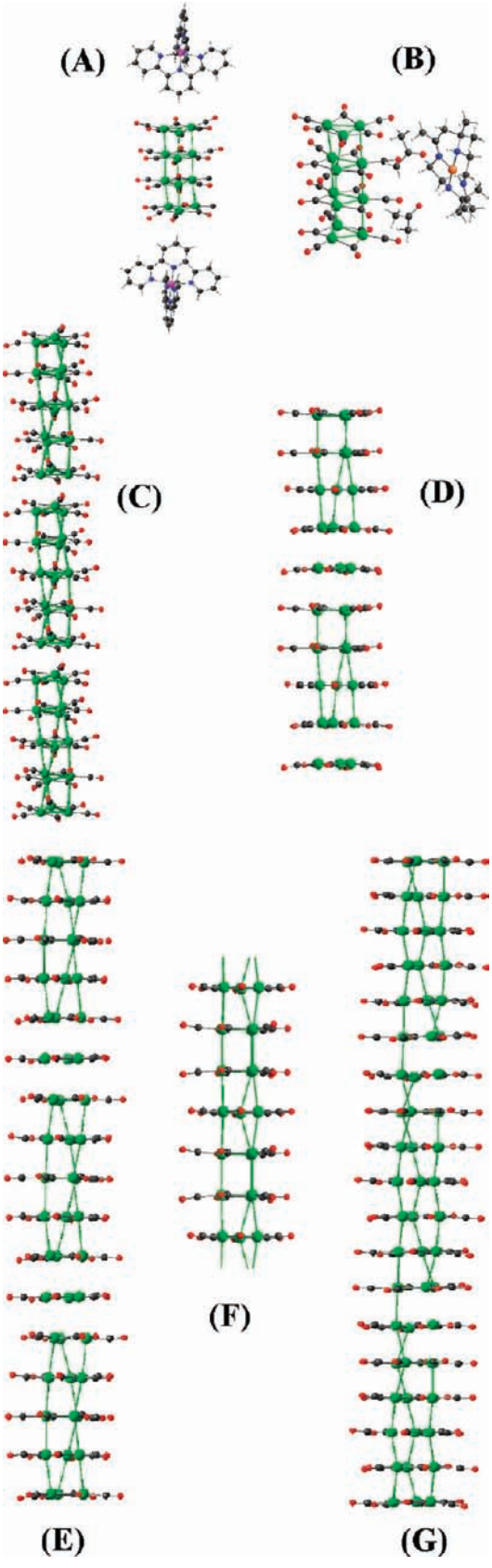

Figure 4. Stacking of the $[Pt_{3n}(CO)_{6n}]^{2-}$ (n = 4−7) anions in (A) $[Ru(tpy)_2][Pt_{12}(CO)_{24}]\cdot 4CH_3COCH_3$, (B) $[Ni(macro)][Pt_{12}(CO)_{24}]\cdot 2CH_3COCH_3$, (C) $[Ru(tpy)_2][Pt_{15}(CO)_{30}]\cdot 3DMF$, (D) $[Ru(bpy)_3][Pt_{15}(CO)_{30}]\cdot 3CH_3COCH_3$, (E) $[Ru(bpy)_3][Pt_{18}(CO)_{36}]$, (F) $[Ru(bpy)_2(2\text{-}PTZ)]_2[Pt_{18}(CO)_{36}]$, and (G) $[Ru(tpy)_2][Pt_{21}(CO)_{42}]\cdot 2DMF$. Pt−Pt bonds are drawn arbitrarily up to 3.34 Å.

chains of $[Ru(tpy)_2][Pt_{15}(CO)_{30}]\cdot 3DMF$ are parallel and give rise to a 1-D packing (Figure 5C).

Conversely, in the $[Ru(bpy)_3][Pt_{15}(CO)_{30}]\cdot 3CH_3COCH_3$ salt, the $[Pt_{15}(CO)_{30}]^{2-}$ anions are arranged into infinite (slightly asymmetric) semicontinuous chains (Figure 4D). In fact, four $Pt_3(\mu\text{-}CO)_3(CO)_3$ units are at normal bonding distances [3.01−3.10 Å between their centroids], whereas the fifth unit is farther apart [3.35 Å calculated from the centroids] and is close to the next cluster unit along the chain [3.49 Å calculated from the centroids]. As a result, the infinite cluster chains are composed of alternating $[Pt_{12}(CO)_{24}]^{2-}$ and $Pt_3(\mu\text{-}CO)_3(CO)_3$ units, with the latter being between two consecutive anions. This type of structure can be defined as (asymmetric) semicontinuous in the sense that there is not yet continuity in the Pt−Pt bonding along the chain but the anions start to approach and lose their molecular identity. This points out that even minor variations of the cation can affect the stacking and packing of the cluster anions. A view of the crystal packing along the c axis (Figure 5D) shows that these semicontinuous chains are all parallel (1-D structure) and form hexagonal channels containing the Ru^{II} cations.

$[Pt_{18}(CO)_{36}]^{2-}$. Similarly, even though both $[Ru(bpy)_3][Pt_{18}(CO)_{36}]$ and $[Ru(bpy)_2(2\text{-}PTZ)]_2[Pt_{18}(CO)_{36}]$ salts are based on infinite stacks of $[Pt_{18}(CO)_{36}]^{2-}$ anions, these form symmetric semicontinuous chains in the former (Figure 4E) and continuous ones in the latter (Figure 4F). In the case of $[Ru(bpy)_3][Pt_{18}(CO)_{36}]$, five $Pt_3(\mu\text{-}CO)_3(CO)_3$ units within the $[Pt_{18}(CO)_{36}]^{2-}$ anion display normal distances between the centroids in the range 3.04−3.11 Å, comparable to the ones reported for $[Ru(bpy)_3][Pt_{15}(CO)_{30}]\cdot 3CH_3COCH_3$ and indicative of direct metal−metal bonds. The sixth $Pt_3(\mu\text{-}CO)_3(CO)_3$ unit, conversely, is shared by two consecutive anions; in fact, its centroid displays distances of 3.26 and 3.28 Å, respectively, from the two neighboring anions (Figure 4E). The corresponding Pt−Pt distances between this $Pt_3(\mu\text{-}CO)_3(CO)_3$ unit and the two adjacent anions are 3.31−3.42 Å, in the limiting region between weakly bonding and nonbonding. Thus, the identity of the single $[Pt_{18}(CO)_{36}]^{2-}$ anions is lost, resulting in infinite symmetric semicontinuous chains composed of perfectly alternating $[Pt_{15}(CO)_{30}]^{2-}$ anions and $Pt_3(\mu\text{-}CO)_3(CO)_3$ units.

Conversely, the $[Pt_{18}(CO)_{36}]^{2-}$ anions of $[Ru(bpy)_2(2\text{-}PTZ)]_2[Pt_{18}(CO)_{36}]$ form infinite continuous chains (Figure 4F), displaying almost identical distances between the centroids of the triangular units [3.11−3.12 Å], as was previously found in $[NMe_4]_2[Pt_{18}(CO)_{36}]\cdot 2CH_3COCH_3$ [3.08−3.09 Å].[10] For both $[Ru(bpy)_3][Pt_{18}(CO)_{36}]$ and $[Ru(bpy)_2(L\text{-}L)]_2[Pt_{18}(CO)_{36}]$ salts, the chains of $[Pt_{18}(CO)_{36}]^{2-}$ anions are parallel (Figure 5E,F). The 1-D packing of $[Ru(bpy)_3][Pt_{18}(CO)_{36}]$ is further organized into hexagonal channels.

$[Pt_{21}(CO)_{42}]^{2-}$. The $[Ru(tpy)_2][Pt_{21}(CO)_{42}]\cdot 2DMF$ salt can be described as a 1-D packing of infinite cluster chains (Figure 4G), all parallel and generating hexagonal channels, inside which are located the cations (Figure 5G). The description of a chain of the $[Pt_{21}(CO)_{42}]^{2-}$ anions is rather complex. In fact, six of the seven $Pt_3(\mu\text{-}CO)_3(CO)_3$ units display normal bonding distances between the centroids [2.96−3.10 Å], as is usually found in the molecular $[Pt_{3n}(CO)_{6n}]^{2-}$ species. The seventh unit is 3.20 Å apart from one anion and 3.46 Å from the following one. Thus, while it is

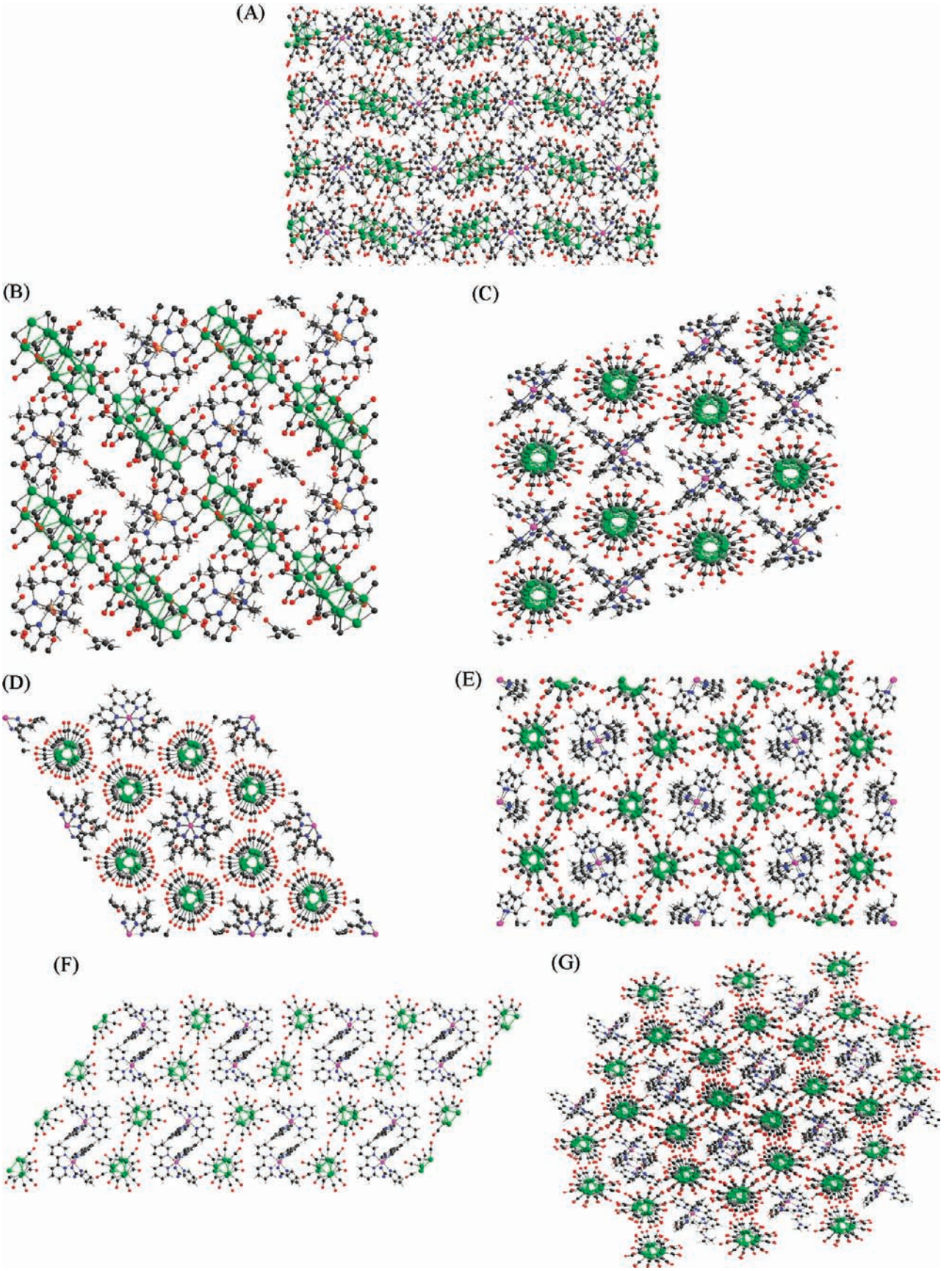

Figure 5. Crystal packing of (A) $[Ru(tpy)_2][Pt_{12}(CO)_{24}]\cdot 4CH_3COCH_3$ (view along the *a* axis), (B) $[Ni(macro)][Pt_{12}(CO)_{24}]\cdot 2CH_3COCH_3$ (view along the *a* axis), (C) $[Ru(tpy)_2][Pt_{15}(CO)_{30}]\cdot 3DMF$ (view along the *a* axis), (D) $[Ru(bpy)_3][Pt_{15}(CO)_{30}]\cdot 3CH_3COCH_3$ (view along the *c* axis), (E) $[Ru(bpy)_3][Pt_{18}(CO)_{36}]$ (view along the *a* axis), (F) $[Ru(bpy)_2(2\text{-}PTZ)]_2[Pt_{18}(CO)_{36}]$ (view along the *b* axis), and (G) $[Ru(tpy)_2][Pt_{21}(CO)_{42}]\cdot 2DMF$ (view along the main axis of the hexagonal channels).

Table 2. Relevant Bonding Parameters (Å) for $[Ru(tpy)_2][Pt_{12}(CO)_{24}]\cdot 4CH_3COCH_3$, $[Ni(macro)][Pt_{12}(CO)_{24}]\cdot 2CH_3COCH_3$, $[Ru(tpy)_2][Pt_{15}(CO)_{30}]\cdot 3DMF$, $[Ru(bpy)_3][Pt_{15}(CO)_{30}]\cdot 3CH_3COCH_3$, $[Ru(bpy)_3][Pt_{18}(CO)_{36}]$, $[Ru(bpy)_2(2\text{-}PTZ)]_2[Pt_{18}(CO)_{36}]$, and $[Ru(tpy)_2][Pt_{21}(CO)_{42}]\cdot 2DMF$

	Pt−Pt intratriangular[a]	Pt−Pt intertriangular[a]	intertriangular distances between the centroids[b]	Pt−Pt contacts between consecutive anions[c]	distances between the centroids of two consecutive anions[d]	stacking
$[Ru(tpy)_2][Pt_{12}(CO)_{24}]\cdot 4CH_3COCH_3$	2.66−2.67	3.02−3.06	3.02−3.05			none
$[Ni(macro)][Pt_{12}(CO)_{24}]\cdot 2CH_3COCH_3$	2.65−2.66	3.02−3.14	3.01−3.06			none
$[Ru(tpy)_2][Pt_{15}(CO)_{30}]\cdot 3DMF$	2.64−2.68	3.03−3.23	2.98−3.09	3.51−3.59	3.58	discontinuous
$[Ru(bpy)_3][Pt_{15}(CO)_{30}]\cdot 3CH_3COCH_3$	2.65−2.66	3.09−3.10	3.01−3.10	3.40−3.54	3.35, 3.49	asymmetric semicontinuous
$[Ru(bpy)_3][Pt_{18}(CO)_{36}]$	2.65−2.67	3.08−3.22	3.04−3.11	3.31−3.42	3.26, 3.28	symmetric semicontinuous
$[Ru(bpy)_2(2\text{-}PTZ)]_2[Pt_{18}(CO)_{36}]$	2.65−2.66	3.12−3.24	3.11−3.12	3.12−3.24	3.11, 3.12	continuous
$[Ru(tpy)_2][Pt_{21}(CO)_{42}]\cdot 2DMF$	2.65−2.68	3.01−3.23	2.96−3.10	3.19−3.68	3.20, 3.46	asymmetric semicontinuous

[a] Pt−Pt distances (range) measured for a molecular anion. [b] Distances (range) between the centroids of the Pt_3 units comprised within a molecular anion. [c] Pt−Pt distances (range) between the outer Pt_3 units of consecutive anions for discontinuous chains; distances (range) between consecutive $[Pt_{3(n-1)}(CO)_{6(n-1)}]^{2-}$ and $[Pt_3(CO)_6]$ units for semicontinuous chains; the same values as Pt−Pt intertriangular for continuous chains. [d] Distances between the centroids of the outer Pt_3 units of consecutive anions for discontinuous chains; distances between consecutive $[Pt_{3(n-1)}(CO)_{6(n-1)}]^{2-}$ and $[Pt_3(CO)_6]$ units for semicontinuous chains; the same values as Pt−Pt intertriangular for continuous chains.

possible to individualize each $[Pt_{21}(CO)_{42}]^{2-}$ anion within the chain, its most external triangular unit is partially shared with the following anion. As a result, the chains of $[Pt_{21}(CO)_{42}]^{2-}$ anions can be described as having a rather asymmetric semicontinuous structure, somehow approaching a discontinuous morphology.

3. General Remarks on the Crystal Structures. Several structural determinations of salts with different mono-[10] and divalent cations containing the $[Pt_{3n}(CO)_{6n}]^{2-}$ (n = 2−8) anions are now available. Considering the arrangement of the cluster anions, all of these structures can be classified within two general categories: (1) nonorganized structures (0-D), where the anions do not form stacks nor chains; (2) organized structures (1-D, 2-D, or 3-D), where the cluster anions are stacked and form chains as long as the macroscopic dimensions of the crystal. Considering a single chain of clusters, this can be continuous, semicontinuous, or discontinuous. Semicontinuous chains can be symmetrical or unsymmetrical. Both display an alternation of $[Pt_{3(n-1)}(CO)_{6(n-1)}]^{2-}$ anions and $Pt_3(CO)_6$ units (the assignment of the negative charge to the $[Pt_{3(n-1)}(CO)_{6(n-1)}]^{2-}$ cluster moiety is due to the fact that previous theoretical calculations showed that these two electrons are needed to form the intertriangular Pt−Pt bonds).[25,26] Thus, semicontinuous structures can be viewed as Lewis adducts of the neutral $Pt_3(CO)_6$ Lewis acid interacting with two adjacent $[Pt_{3(n-1)}(CO)_{6(n-1)}]^{2-}$ Lewis bases. In the symmetrical semicontinuous chains (e.g., $[Ru(bpy)_3][Pt_{18}(CO)_{36}]$ and $[NBu_4]_2[Pt_{24}(CO)_{48}]$),[10] the $Pt_3(CO)_6$ moiety is equidistant from the two adjacent $[Pt_{3(n-1)}(CO)_{6(n-1)}]^{2-}$ cluster units. Conversely, in the asymmetrical ones (e.g., $[Ru(bpy)_3][Pt_{15}(CO)_{30}]\cdot 3CH_3COCH_3$ and $[Ru(tpy)_2][Pt_{21}(CO)_{42}]\cdot 2DMF$), the $Pt_3(CO)_6$ moiety is regularly closer to one of the two. From this point of view, the above situation is reminiscent and somehow related to that displayed by miscellaneous salts of the $[FHF]^-$ anion.[27]

The formation of infinite continuous platinum chains, based on stacked $\{Pt_3(CO)_6\}$ units, was predicted by Hoffmann and co-workers several years ago.[25] The possibility that such 1-D chains could show Peierls distortions, owing to a partial filling of the energy band arising from the overlap of the cyclopropenyl-like lowest unoccupied molecular orbitals of the $\{Pt_3(CO)_6\}$ units along the pseudo-C_3 axis, was also advanced. In the case where the stack is generated by the assembly of $[Pt_{3n}(CO)_{6n}]^{2-}$ ($n > 1$) cluster dianions, the above molecular orbital band would only be $1/n$ filled.[28] The fact that semicontinuous and continuous chains have also been experimentally found indicates that other factors are also operative in determining the finest details of the final crystal structures. In principle, the introduction of nonbonding gaps between the anions along a chain might result in a loss of density, which would destabilize the structure, making a more compact structure (continuous chain) preferable. That, however, might be contrasted by electronic stabilization via Peierls distortions, as well as by the electrostatic repulsions between anions along the chain.

It seems conceivable to think that lower-nuclearity $[Pt_{3n}(CO)_{6n}]^{2-}$ ($n \leq 4$) clusters always crystallize into 0-D structures, probably because of a large electrostatic repulsion hampering anion stacking. As the nuclearity increases, with the negative charge per cluster being constant, electrostatic repulsions decrease and the anions can begin to approach the formation of chains. At this stage, the size of the cation and the reciprocal repulsion between them may become important in determining the crystal structure. For the same $[Pt_{3n}(CO)_{6n}]^{2-}$ ($n \geq 5$) anion, larger cations favor discontinuous or semicontinuous chains, whereas smaller ones enable the formation of semicontinuous or even continuous chains. This point is nicely exemplified by the arrangement of the $[Pt_{18}(CO)_{36}]^{2-}$ anions in $[Ru(bpy)_3][Pt_{18}(CO)_{36}]$ (symmetric semicontinuous chains) versus $[NMe_4]_2[Pt_{18}(CO)_{36}]\cdot 2CH_3COCH_3$ (continuous chains)[10] or the $[Pt_{24}(CO)_{48}]^{2-}$ anions in

(25) Underwood, D. J.; Hoffmann, R.; Tatsumi, K.; Nakamura, A.; Yamamoto, Y. *J. Am. Chem. Soc.* **1985**, *107*, 5968.
(26) Mealli, C. *J. Am. Chem. Soc.* **1985**, *107*, 2245.
(27) Wells, A. F. *Structural Inorganic Chemistry*; Oxford Science Publications: Oxford, U.K., 1987.
(28) (a) Whangbo, M.-H. *Acc. Chem. Res.* **1983**, *16*, 95. (b) Burdett, J. K. *Chemical Bonding in Solids*; Oxford University Press: New York, 1995; pp 48−65.

Table 3. Effect of the L/D^* Ratio on the Crystal Packing of $[Pt_{3n}(CO)_{6n}]^{2-}$ ($n = 4-8$) Anions with Different Mono- and Dications

compound	L (Å)[a]	D (Å)[b]	L/D^*[c]	packing	stacking	ref
$[Ru(tpy)_2][Pt_{12}(CO)_{24}]\cdot 4CH_3COCH_3$	12.6	13.9	0.91	0-D	none	this work
$[NBu_4]_2[Pt_{12}(CO)_{24}]$	12.6	12.2	0.52	0-D	none	10
$[Ni(macro)][Pt_{12}(CO)_{24}]\cdot 2CH_3COCH_3$	12.6	12.3	1.02	0-D	none	this work
$[NMe_4]_2[Pt_{12}(CO)_{24}]$	12.6	5.0	1.26	0-D	none	10
$[Ru(tpy)_2][Pt_{15}(CO)_{30}]\cdot 3DMF$	15.9	13.9	1.14	1-D	discontinuous	this work
$[NEt_4]_2[Pt_{15}(CO)_{30}]$	15.9	7.9	1.01	3-D	discontinuous	10
$[Ru(bpy)_3][Pt_{15}(CO)_{30}]\cdot 3CH_3COCH_3$	16.1	13.9	1.16	1-D	asymmetric semicontinuous	this work
$[Ru(bpy)_3][Pt_{18}(CO)_{36}]$	19.0	13.9	1.37	1-D	symmetric semicontinuous	this work
$[NMe_4]_2[Pt_{18}(CO)_{36}]\cdot 2CH_3COCH_3$	18.9	5.0	1.89	1-D	continuous	10
$[Ru(tpy)_2][Pt_{21}(CO)_{42}]\cdot 2DMF$	21.7	13.9	1.56	1-D	asymmetric semicontinuous	this work
$[NEt_4]_2[Pt_{24}(CO)_{48}]$	24.9	7.9	1.58	2-D	continuous	10
$[NBu_4]_2[Pt_{24}(CO)_{48}]$	24.9	12.2	0.98	2-D	symmetric semicontinuous	10
$[Ru(bpy)_2(2\text{-PTZ})]_2[Pt_{18}(CO)_{36}]$	19.0	14.0	0.68	1-D	continuous	this work

[a] L = (distance between the centroids of the outer Pt_3 triangles) + [2(van der Waals radius of Pt)]. [b] For the cations presented in this work, D = [2(average distance between the ruthenium (or nickel) and hydrogen atoms of the outer aromatic ring (or CH_3))] + [2(van der Waals radius of H)]; for $[NR_4]^+$ cations, D = [2(average distance between the nitrogen and hydrogen atoms of the outer $-CH_3$ moiety)] + [2(van der Waals radius of hydrogen)]. [c] $D^* = Dy$, where y = number of cations per cluster anion ($y = 2$ for monocations; $y = 1$ for dications).

$[NBu_4]_2[Pt_{24}(CO)_{48}]$ (symmetric semicontinuous chains) versus $[NEt_4]_2[Pt_{24}(CO)_{48}]$ (continuous chains).[10]

It may be, therefore, concluded that miscellaneous electronic, electrostatic, and steric factors contribute to the final crystal structures of the $[M]_y[Pt_{3n}(CO)_{6n}]$ ($n = 2-8$; $y = 1, 2$) salts (0-D, 1-D, 2-D, 3-D; discontinuous, semicontinuous, continuous). A single parameter that seems to partially rationalize (but not fully predict) the resulting structures is the L/D^* ratio (L = length of the cluster anion; D = diameter of the cation; $D^* = Dy$; y = number of cations per anion). The L/D^* ratios of all pertinent structures are compared with the experimental morphologies of chains in Table 3. Compared to our previous paper in which this parameter was introduced,[10] herein the diameter of the cation (D) has been multiplied by the number of cations per single anion in order to account for the different stoichiometries of the salts. This results in halved values of L/D^* for monocations compared to those previously reported[10] and makes these values directly comparable to those herein found for divalent cations.

As shown, in the case of $[NR_4]^+$ monocations[10] as well as divalent cations such as $[Ni(macro)]^{2+}$, $[Ru(tpy)_2]^{2+}$, and $[Ru(bpy)_3]^{2+}$, L/D^* ratios ≥ 1.5 favor the self-assembly of $[Pt_{3n}(CO)_{6n}]^{2-}$ ($n \geq 6$) dianions into infinite continuous wires because squeezing together these elongated dianions does not trigger too high repulsive forces. Because repulsive forces are expected to increase rapidly for $n < 6$, L/D^* ratios comprised of the 1−1.5 range are less discriminating and may lead to 0-D packing or semicontinuous and discontinuous wires that are dependent on the length of the dianion. Conversely, L/D^* ratios <1 usually result in 0-D structures.

The major apparent exception to the above-mentioned rules is represented by $[Ru(bpy)_2(2\text{-PTZ})]_2[Pt_{18}(CO)_{36}]$ ($L/D^* = 0.68$). In this salt, there are present continuous chains even if the L/D^* ratio is significantly less than 1 and it contains the $[Ru(bpy)_2(2\text{-PTZ})]^+$ monocation, which is as bulky as the $[Ru(tpy)_2]^{2+}$ and $[Ru(bpy)_3]^{2+}$ dications. It may be speculated that such an exception is made possible by the adoption of a packing based on the alternation of layers made of aligned continuous chains of $[Pt_{18}(CO)_{36}]^{2-}$ dianions and layers of $[Ru(bpy)_2(2\text{-PTZ})]^+$ monocations interlaced by $\pi-\pi$ interactions of the aromatic rings (see Figure 5F).

4. Electrical Resistivity. Electrical resistivity measurements on pressed pellets of crystalline samples of $[Ru(tpy)_2][Pt_{12}(CO)_{24}]\cdot 4CH_3COCH_3$, $[Ni(macro)][Pt_{12}(CO)_{24}]\cdot 2CH_3COCH_3$, $[Ru(tpy)_2][Pt_{15}(CO)_{30}]\cdot 3DMF$, $[Ru(bpy)_3][Pt_{18}(CO)_{36}]$, and $[Ru(tpy)_2][Pt_{21}(CO)_{42}]\cdot 2DMF$ have been performed with a four-point probe. Their values are compared in Table 4 with those of $[NBu_4]_2[Pt_{12}(CO)_{24}]$, $[NMe_4]_2[Pt_{12}(CO)_{24}]$, $[NEt_4]_2[Pt_{15}(CO)_{30}]$, $[NMe_4]_2[Pt_{18}(CO)_{36}]\cdot 2CH_3COCH_3$, $[NEt_4]_2[Pt_{24}(CO)_{48}]$, and $[NBu_4]_2[Pt_{24}(CO)_{48}]$ previously determined.[10] Conversely, $[Ru(bpy)_3][Pt_{15}(CO)_{30}]\cdot 3CH_3COCH_3$ and $[Ru(bpy)_2(2\text{-PTZ})]_2[Pt_{18}(CO)_{36}]$ have not been measured because they were always obtained in an insufficiently pure form. Unfortunately, measurements on single crystals have been hindered by the fragility of the whiskers shown in Figure 1 combined with the necessity to carry out handling and experiments in an inert atmosphere.

Resistivity measurements clearly point out that the resemblance of the infinite $Pt_3(CO)_3(\mu\text{-}CO)_3$ stacks found in continuous chains to CO-insulated platinum cables is not only morphological but also functional. Whereas 0-D salts expectedly display the resistivity of an insulator material ($\geq 10^8$ Ω cm), the salts that are based on discontinuous, semicontinuous, or continuous stacks (1-D, 2-D, or 3-D) exhibit resistivity decreasing from 10^6 to 10^2 Ω cm. Typical values are 10^5-10^6, ca. 10^4, and ca. 10^2 Ω cm for discontinuous, semicontinuous, or continuous chains, respectively, indicating that the electrical conductivity increases as the cluster anions approach and delocalized Pt−Pt bonds extend along the whole chain. It seems reasonable to think that in polycrystalline pressed pellets the electrons must hop from grain-to-grain and a resistance could develop as a function of the number, size, and orientation of the grains. It appears, therefore, rather remarkable that a relationship between the electrical resistivity and interanionic gap could be clearly noticeable within homogeneous categories, whereas the effect of

Table 4. Dependence of the Resistivity from the Crystal Packing and Interanionic Gap

compound	L/D*	packing	gap[a] [Å]	resistivity [Ω cm]	ref
$[Ru(tpy)_2][Pt_{12}(CO)_{24}]\cdot 4CH_3COCH_3$	0.91	0-D		$>10^8$	this work
$[NBu_4]_2[Pt_{12}(CO)_{24}]$	0.52	0-D		$>10^8$	10
$[Ni(macro)][Pt_{12}(CO)_{24}]\cdot 2CH_3COCH_3$	1.02	0-D		$>10^8$	this work
$[NMe_4]_2[Pt_{12}(CO)_{24}]$	1.26	0-D		$>10^8$	10
$[Ru(tpy)_2][Pt_{15}(CO)_{30}]\cdot 3DMF$	1.14	1-D	3.58	3×10^6	this work
$[NEt_4]_2[Pt_{15}(CO)_{30}]$	1.01	3-D	3.50	2×10^5	10
$[Ru(bpy)_3][Pt_{18}(CO)_{36}]$	1.37	1-D	3.28	1.5×10^4	this work
$[NMe_4]_2[Pt_{18}(CO)_{36}]\cdot 2CH_3COCH_3$	1.89	1-D	3.08	6×10^2	10
$[Ru(tpy)_2][Pt_{21}(CO)_{42}]\cdot 2DMF$	1.56	1-D	3.46	6.5×10^4	this work
$[NEt_4]_2[Pt_{24}(CO)_{48}]$	1.58	2-D	3.07	1×10^2	10
$[NBu_4]_2[Pt_{24}(CO)_{48}]$	0.98	2-D	3.21	2×10^3	10

[a] The gap between $[Pt_{3n}(CO)_{6n}]^{2-}$ dianions along the stack is given in angstroms: the distance between the centroids of the external Pt_3 units of two consecutive anions is used for discontinuous chains; the longer distance between the centroids of consecutive $[Pt_{3(n-1)}(CO)_{6(n-1)}]^{2-}$ and $[Pt_3(CO)_6]$ units is used for semicontinuous chains; the longest distance between the centroids of two consecutive $[Pt_3(CO)_6]$ units is used for continuous chains.

1-D, 2-D, or 3-D packing is less clear-cut. Thus, reduction of the gap from 3.58 to 3.50 Å in discontinuous $[Ru(tpy)_2][Pt_{15}(CO)_{30}]\cdot 3DMF$ and $[NEt_4]_2[Pt_{15}(CO)_{30}]$[10] results in a variation of the resistivity of 1 order of magnitude (from 3×10^6 to 2×10^5 Ω cm). Analogously, semicontinuous systems [e.g., $[Ru(tpy)_2][Pt_{21}(CO)_{42}]\cdot 2DMF$ (gap 3.46 Å), $[Ru(bpy)_3][Pt_{18}(CO)_{36}]$ (gap 3.28 Å), and $[NBu_4]_2[Pt_{24}(CO)_{48}]$[10] (gap 3.21 Å)] point out an evident dependence of the resistivity (6.5×10^4, 1.5×10^4, and 2×10^3 Ω cm, respectively) from the gap. These data also suggest that the nuclearity of the cluster has little, if any, influence on the resistivity. This is also confirmed by the fact that salts based on the same $[Pt_{3n}(CO)_{6n}]^{2-}$ anions can have very different resistivities based on the continuity of the chains and the interanionic gaps.

5. DLS Studies. The miscellaneous modes of the self-assembly of $[Pt_{3n}(CO)_{6n}]^{2-}$ anions in the solid state documented here seem to be relevant also in explaining some of their previously reported behavior in solution. For instance, the symmetrical and unsymmetrical semicontinuous chains, in which $\{Pt_3(CO)_6\}$ units are shared by contiguous $[Pt_{3(n-1)}(CO)_{6(n-1)}]^{2-}$ anions, seem to represent snapshots in the solid state of the intermolecular exchange of $\{Pt_3(CO)_6\}$ units, which was detected in solution by ^{195}Pt NMR spectroscopy of mixtures of $[Pt_9(CO)_{18}]^{2-}$ and $[Pt_{12}(CO)_{24}]^{2-}$.[29] That and the finding that the $[Pt_{3n}(CO)_{6n}]^{2-}$ dianions with $n > 4$ are silent in ^{195}Pt NMR experiments fueled interest in investigating possible self-assembly phenomena in solution. Indeed, in principle, the intermolecular exchange of $Pt_3(CO)_6$ units in solution may occur via either a dissociative or associative mechanism. The dissociative mechanism will require shuttling of an outer $Pt_3(CO)_6$ unit between two either different or identical $[Pt_{3n}(CO)_{6n}]^{2-}$ molecular ions. An associative mechanism might imply the self-assembly of two or more $[Pt_{3n}(CO)_{6n}]^{2-}$ anions into a supramolecular aggregate, such as a chunk of a chain, followed by its falling apart. A wide distribution in the size of such purported supramolecular aggregates and their slow tumbling in solution can smear out any NMR signal.

DLS appeared particularly attractive to gather information on this point because it is experimentally simple, can be applied to almost any kind of sample, and is completely noninvasive.[7] It has, however, the limit to measure the hydrodynamic diameter of all species present in solution without giving any chemical information.

Preliminary DLS measurements on CH_3CN solutions of $[NBu_4]_2[Pt_{15}(CO)_{30}]$ and $[NBu_4]_2[Pt_{18}(CO)_{36}]$ showed only minor differences between the two samples. Therefore, only the spectra of the latter are shown and discussed in some detail. Solutions of $[NBu_4]_2[Pt_{18}(CO)_{36}]$ (0.1−0.2 wt % in CH_3CN) systematically showed the presence of particles with huge hydrodynamic diameters ranging from 40 nm up to ca. 6 μm, as shown, for instance, in Figure 6a. The initial correlation coefficient (0.9−1) was comparable to that of a suspension of latex nanoparticles used as the standard (nominal diameter 66 nm; correlation coefficient ca. 1).

Inspection of the commercial CH_3CN used as the solvent pointed out that it often contains small amounts of the hugest nanoparticles (700−6000 nm), whereas the particles displaying diameters in the 50−800 nm range were more likely originating from $[NBu_4]_2[Pt_{18}(CO)_{36}]$. To avoid spurious contaminations arising from nanoparticles introduced either by the solvent or impurities in the $[NBu_4]_2[Pt_{18}(CO)_{36}]$ sample, the above solution was filtered with a nanometric (100 nm) filter. The filtered solution was stored in a sealed DLS cuvette and monitored as soon as filtered and after 12 h of standing (parts b and c of Figure 6, respectively).

DLS spectra of freshly filtered solutions display a situation rapidly evolving with time. This is exemplified by the spectra of the two consecutive runs reported in Figure 6b [first run in blue, second run (after a few minutes) in black]. It seems, however, rewarding that the great majority of particles present in the acetonitrile solution of $[NBu_4][Pt_{18}(CO)_{36}]$ as soon as filtered displays a nominal hydrodynamic diameter centered at ca. 2 nm [see, in particular, the first run (blue curve) in Figure 6b]. This nicely compares with both the length of the cylinder circumscribing the $[Pt_{18}(CO)_{36}]^{2-}$ dianion (1.91 nm, including the van der Waals radius of platinum), as inferred from its X-ray structure in the solid state, and the diameter of the sphere having a volume equivalent to that of the above cylinder (1.52 nm). The variation with time of the correlation coefficient is yet satisfactory even if its initial value is only about one-third of that of the original solution. It seemed likely that the drop of the initial correlation coefficient could be due to a significant decrease of the concentration of the solution as a consequence of

(29) (a) Brown, C.; Heaton, B. T.; Chini, P.; Fumagalli, A.; Longoni, G. *J. Chem. Soc., Chem. Commun.* **1977**, 309. (b) Brown, C.; Heaton, B. T.; Towl, A. D. C.; Chini, P.; Fumagalli, A.; Longoni, G. *J. Organomet. Chem.* **1979**, *181*, 233.

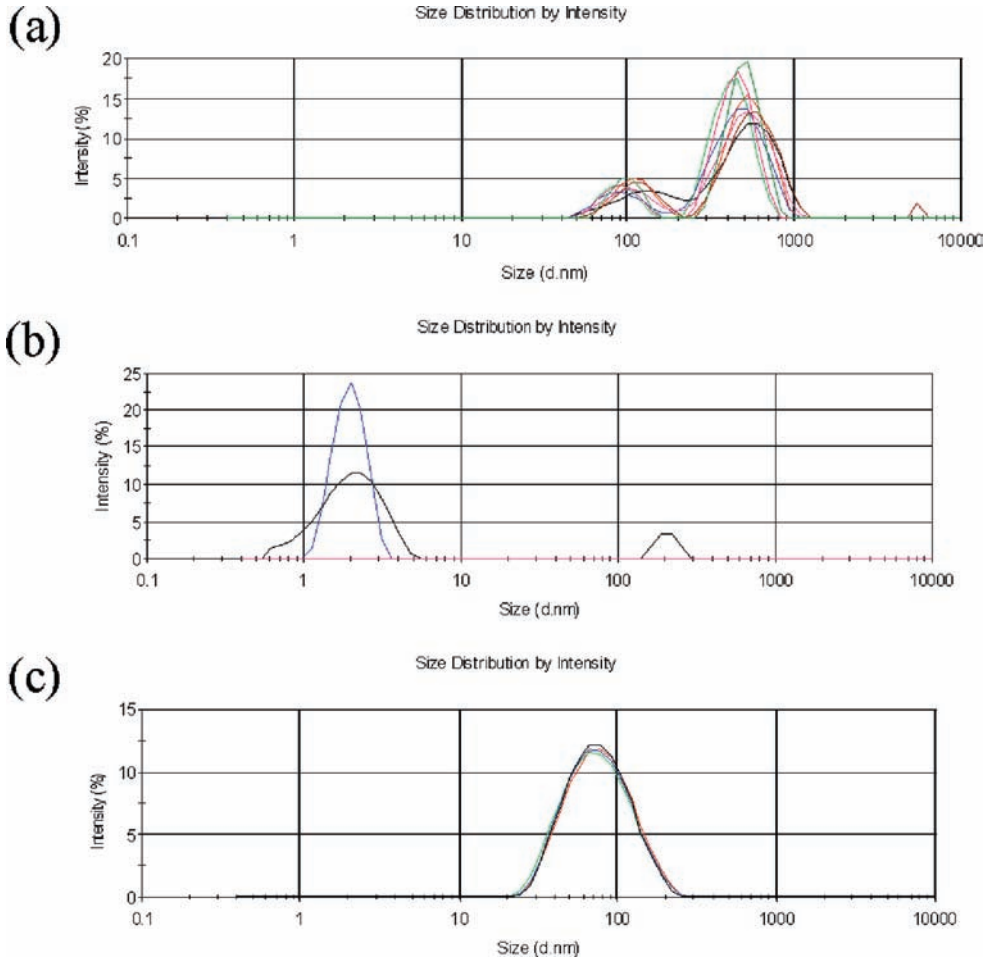

Figure 6. Size distribution (in the intensity) of nanoparticles present at 20 °C in a CH_3CN solution of $[NBu_4]_2[Pt_{18}(CO)_{36}]$ (nominally 0.2% wt) (a), as soon as filtered with a 100 nm filter (b), and after 12 h equilibration from filtration (c).

filtration with a 100 nm filter. As confirmed by platinum analysis, filtration removes a significant part of the sample and, as a consequence, the real concentration of the solution is much lower than the nominal one. Besides, filtration with a 20 nm filter of the solution of Figure 6 gives rise to signals displaying even lower initial correlation coefficients (ca. 0.1) and ill-defined correlation functions, as a result of a further decrease in the concentration of the sample.

The rapid evolution of the situation is well represented by a comparison of the two spectra of Figure 6b registered a few minutes one after the other. In particular, the second run (black curve) displays a peak centered at ca. 2 nm broader than the one of the first run, as well as a weak feature at 250 nm. After 12 h of standing in a sealed cuvette, the solution of Figure 6b displays the yet different DLS profile shown in Figure 6c. Only huge nanoparticles with broad size distributions centered in the 69−80 nm range are detectable. The correlation functions of the above spectra are good and do not change after the measurement was repeated several times. However, the initial correlation coefficient is again approximately one-third of that of latex nanoparticles used as standards.

The presently available data might have the following interpretation. The hydrodynamic diameters observed in Figure 6a might indicate that a significant part of $[NBu_4]_2[Pt_{18}(CO)_{36}]$ (as well as $[NBu_4]_2[Pt_{15}(CO)_{30}]$) dissolves in acetonitrile as supramolecular aggregates or variable chunks of their ionic lattice in a solvent cage rather than solvated $[NBu_4]^+$ and $[Pt_{18}(CO)_{36}]^{2-}$ ions. The latter ion is only detectable in solution (Figure 6b) upon elimination of the former aggregates and spurious particles by nanofiltration. Finally, the profile of the solution after 12 h of standing (Figure 6c) points out the occurrence in solution of significant reaggregation in very large nanoparticles. The hydrodynamic diameters shown in Figure 6c might be justified by aggregation in solution of at least 30 $[Pt_{18}(CO)_{36}]^{2-}$ dianions in a solvent cage. Partially in keeping with this suggestion, the hydrodynamic diameter of the observable nanoparticles in equilibrated solutions increases upon an increase in the initial nominal concentration and/or a decrease in the temperature to 2 °C. The lack of any detectable ^{195}Pt NMR signal of comparably or more concentrated $[NBu_4]_2[Pt_{18}(CO)_{36}]$ solutions hinders all attempts to gather more chemical information on the above purported aggregation. Related attempts to prove aggregation by pulsed field gradient spin−echo (PGSE) NMR studies of the protons of the cation have likewise been completely unsuccessful.

As an alternative explanation, one could think that the huge nanoparticles observed at the beginning of the experiment and in time-equilibrated samples might be due to partial cluster decomposition into colloidal carbonylated platinum nanoparticles. This latter interpretation,

however, seems less likely because no color change was observed during DLS measurements and, consistently, no significant change in the IR spectra of the solutions before and after DLS experiments has ever been observed.

As a final albeit necessary word of care, it must be taken into account that the DLS intensity is proportional to D^6 (D = hydrodynamic diameter). Therefore, even relatively few particles with a large D would give rise to intense DLS signals, which could hide those particles having sizes comparable with those of molecular $[Pt_{15}(CO)_{30}]^{2-}$ and $[Pt_{18}(CO)_{36}]^{2-}$ dianions. It seems, therefore, wise to postpone any definite conclusion until this purported aggregation phenomenon is substantiated by a completely independent and complementary technique. Work is in progress on different although related systems that are potentially more amenable to NMR investigations.

Conclusions

The present work confirms the tendency of Chini's clusters $[Pt_{3n}(CO)_{6n}]^{2-}$ to self-assemble in the solid state, yielding different organized structures. This behavior was previously documented for $[NR_4]^+$ monocations.[10] The present work proves a similar behavior of their salts of miscellaneous divalent cations. As an unexpected bonus, the Ru^{II} dication allowed the first structural characterization of the previously unknown $[Pt_{21}(CO)_{42}]^{2-}$ dianion. Thus, now all $[Pt_{3n}(CO)_{6n}]^{2-}$ species with n ranging from 2 to 8 have been structurally determined by single-crystal X-ray diffraction.

Concerning the crystal packing of their salts, and independent of the cations employed, we can conclude that all species with $n \leq 4$ do not form cluster chains and give rise to ionic 0-D structures. This is probably due to electrostatic repulsions between these small and negatively charged anions. As the nuclearity of the cluster increases ($n \geq 5$), with the charge constant being negative, electrostatic repulsions decrease and the cluster anions can approach each other and give rise to infinite chains, which can be discontinuous, semicontinuous, or continuous. The size of the cation is rather important in order to enable one of these three possibilities. For instance, it was previously reported that $[NEt_4]_2[Pt_{24}(CO)_{48}]$ displayed continuous chains, whereas they became semicontinuous in $[NBu_4]_2[Pt_{24}(CO)_{48}]$ because of the larger size of the cation.[10] Similarly, the herein reported $[Ru(bpy)_3][Pt_{18}(CO)_{36}]$ contains semicontinuous chains of $[Pt_{18}(CO)_{36}]^{2-}$ anions, whereas the same anions form continuous chains in $[NMe_4]_2[Pt_{18}(CO)_{36}]\cdot 2Me_2CO$[10] because of the presence of smaller and less charged cations.

A correlation between the crystal packing and the L/D^* ratio for both mono- and dications is evident, even though it is not clear-cut. More interestingly, also a strict relationship between the crystal structure adopted by these salts and their electrical properties as pressed microcrystalline pellets is confirmed. Thus, 0-D structures that contain isolated ions are electrical insulators. Conversely, as soon as chains of cluster anions are present, the electrical resistivity decreases in the following order: discontinuous chains > semicontinuous chains > continuous chains, with typical values of 10^5-10^6, 10^4, and 10^2 Ω cm, respectively. Moreover, when stacks are compared with the same morphology of the chains, the electrical resistivity decreases upon a decrease of the gap between consecutive anions. Elucidation of the mechanism of electrical conduction within these materials will require much future work, fueled by the perspective to assemble molecular circuits. Within a single chain, conduction probably arises from the presence of delocalized molecular orbitals extending over the whole chain. This is in keeping with the observed trend showing that the best conductivity is displayed by continuous chains. Nonetheless, because electrical measurements have been performed on pressed polycrystalline pellets, electron hopping from grain-to-grain should limit the conductivity. In this context, it is worth mentioning that the typical resistivity of a continuous-chain salt is comparable to that of the doped Krogmann salt. For instance, $K_2[Pt(CN)_4]\cdot 0.4Br$ displays a resistivity as pressed pellets of 10^3 Ω cm,[30] which decreases at 10^{-2} Ω cm in single crystals.[31] Unfortunately, all attempts to measure the single-crystal variable-temperature conductivity of whiskers such as those shown in Figure 1 have so far been hindered by their fragility, combined with the necessity to handle the samples under inert conditions.

Finally, even though the conclusion of DLS measurements should be taken with care for the reasons exposed in the previous section, it seems safe to conclude that some aggregation of Chini's clusters already occurs in solution, as a function of the cluster nuclearity, concentration, solvent, and temperature. Indeed, the predictably small $\Delta G°$ of solvation of these anions may favor only the partial disruption of the ionic lattice on solution, whereas progressive reaggregation of the cluster ions upon standing preludes the formation of a crystal seed and crystallization in macroscopic whiskers because the solubility is decreased by diffusion of a nonsolvent. In order to shed further light on this aggregation phenomenon in solution and quantify their relevance, it is, however, unavoidable to wait for parallel experiments carried out via a complementary technique, which could also give some chemical information.

Acknowledgment. We thank the University of Bologna (Project CLUSTERCAT) and MIUR (PRIN2008) for funding.

Supporting Information Available: CIF files giving X-ray crystallographic data for the structure determinations of $[Ru(tpy)_2][Pt_{12}(CO)_{24}]\cdot 4CH_3COCH_3$, $[Ni(macro)][Pt_{12}(CO)_{24}]\cdot 2CH_3COCH_3$, $[Ru(tpy)_2][Pt_{15}(CO)_{30}]\cdot 3DMF$, $[Ru(bpy)_3][Pt_{15}(CO)_{30}]\cdot 3CH_3COCH_3$, $[Ru(bpy)_3][Pt_{18}(CO)_{36}]$, $[Ru(bpy)_2(2\text{-}PTZ)]_2[Pt_{18}(CO)_{36}]$, and $[Ru(tpy)_2][Pt_{21}(CO)_{42}]\cdot 2DMF$. This material is available free of charge via the Internet at http://pubs.acs.org.

(30) Krogmann, K. *Angew. Chem., Int. Ed.* **1969**, *8*, 35.
(31) Zeller, H. R.; Beck, A. *J. Phys. Chem. Solids* **1974**, *35*, 77.